INORGANIC CHEMISTRY







FRONTIERS

RESEARCH ARTICLE

View Article Online
View Journal



Cite this: DOI: 10.1039/d5qi00986c

Star-shaped Pt(II) complexes with excellent optical power limiting performance and their flexible optical limiters†

Lai Hu, Zhiyuan Chen, Zhi Zhao, Ruiqi Chen, Senqiang Zhu, 🕩 * Rui Liu 🕩 * and Hongjun Zhu

Efficient optical power limiting (OPL) materials are crucial for protecting optical devices and the eyes. However, achieving strong OPL responses while maintaining high optical transparency and processability remains a challenge. Herein, we report a molecular design strategy to improve the OPL performance of a series of Pt(III) complexes (**Pt-1a-Pt-2c**) by incorporating trinuclear Pt centers and modulating the coreethynyl ligand electronic interacations. The trinuclear Pt centers extended the triplet-state lifetimes (0.52–2.05 μ s) and enhanced the excited-state absorption (ESA), while the core-ethynyl ligand interacations effectively tuned the ground- and excited-state properties. These complexes exhibited tunable nonlinear optical (NLO) and OPL properties at 532 nm, with a minimum normalized transmittance (T_{min}) in the range of 0.38–0.78. Notably, **Pt-2b** showed outstanding OPL performance with a nonlinear absorption coefficient (β_{eff}) and optical limiting threshold (F_{OL}) of 192.15 cm GW⁻¹ and 0.71 J cm⁻², respectively. In flexible films, **Pt-2b@PDMS-1.00 wt**% demonstrated markedly enhanced OPL performance (β_{eff} = 965.83 cm GW⁻¹, F_{OL} = 0.26 J cm⁻²), surpassing the performance of many reported OPL materials. This study provides valuable insights into designing transparent Pt(II) complexes with superior OPL properties, and highlights the promise of flexible films for photonic applications.

Received 21st April 2025, Accepted 26th June 2025 DOI: 10.1039/d5qi00986c

rsc.li/frontiers-inorganic

Introduction

Nonlinear optical (NLO) materials have garnered significant interest owing to their broad applications in pulsed laser generation, optical power limiting (OPL), optical switching, and bioimaging. OPL materials are particularly valuable as they attenuate high-energy laser pulses to protect sensitive optical devices and the human eyes while maintaining high transmittance for low-energy light. Ideal OPL materials should possess rapid response times, low limiting thresholds, high transparency, and good stability. Currently developed OPL materials include inorganic compounds, organic π -conjugated molecules, organic compounds, organic π -conjugated molecules, organic frameworks (MOFs), organic π -clusters (metal and metal-oxo clusters), organic materials, organic random materials, organic

instance, C_{60} and porphyrins/phthalocyanines show strong OPL activity but suffer from intense absorption in the 400–700 nm visible range, which reduces its transparency. Although, 2D materials offer broadband OPL responses, they often exhibit poor dispersibility, and materials such as black phosphorus also suffer from limited stability. Thus, developing high-performance OPL materials that combine excellent transparency, stability, and processability, along with solid-state OPL limiters that are suitable for diverse applications remains a critical challenge in this field.

Square-planar $Pt(\pi)$ complexes exhibit intriguing photophysical properties²⁹ and have been widely explored in organic light-emitting devices (OLEDs),³⁰ OPL,³¹ organic solar cells,³² and self-assembled materials.³³ Notably, Pt-induced efficient intersystem crossing (ISC) generates long-lived triplet states with high quantum yields, facilitating two-photon absorption (TPA) and reverse saturable absorption (RSA), making them promising candidates for OPL applications.^{34,35} Cyclometalated $Pt(\pi)$ complexes show remarkable OPL performance because of their strong spin–orbit coupling (SOC) effect. However, their intense metal-to-ligand charge transfer (MLCT) and ligand-to-ligand charge transfer (LLCT) transitions reduce their optical transparency.^{29,36} In contrast, alkylphosphine $Pt(\pi)$ complexes exhibit weaker MLCT absorption,

School of Chemistry and Molecular Engineering, Nanjing Tech University, Nanjing 211816, China. E-mail: zhusenqiang1993@njtech.edu.cn, rui.liu@njtech.edu.cn

† Electronic supplementary information (ESI) available. CCDC: 2288730–2288732 and 2213945. For ESI and crystallographic data in CIF or other electronic format see DOI: https://doi.org/10.1039/d5qi00986c

ensuring better transparency, and phosphine ligands (PR₃) improve solubility. In recent years, Schanze and Zhou et al. have reported numerous alkylphosphine Pt(II) acetylides and Pt(II) polyynes with considerable TPA and RSA effects, successfully demonstrating their OPL applications.^{37–41} Some of these molecular systems even outperform C₆₀ and metalloporphyrins. However, current studies remain focused on linear structures. The weak Pt d_{π} - π orbital mixing limits their OPL activity. Thus, achieving strong OPL responses while maintaining high transparency remains a critical challenge that urgently needs to be addressed in this field.

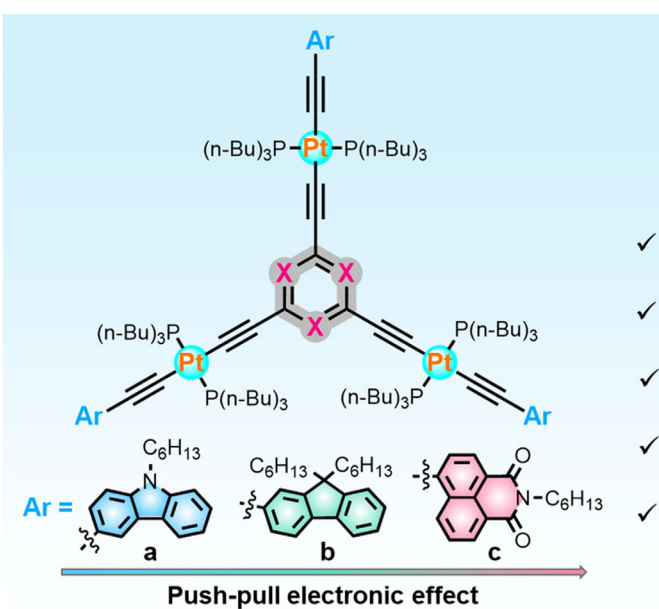
Star-shaped Pt(II) structures are promising candidates to enhance the OPL performance of alkylphosphine Pt(II) complexes, with several advantages, such as (1) synergistic interactions among the branches improve the nonlinear polarizability (χ) ; ^{42,43} (2) trinuclear Pt centers introduce strong SOC effects, promoting ISC and enhancing excited-state absorption (ESA);⁴⁴ and (3) compared with Pt(II)-based dendrimers, star-shaped Pt(II) complexes are more synthetically accessible and cost-effective. 45 For example, Zhou et al. reported that in V-shaped and star-shaped Pt (II) acetylide systems, high-density Pt centers efficiently enhanced the SOC effect, improving the OPL activity. 46 Some Pt(II) acetylides even surpassed C₆₀ in OPL performance while maintaining high transparency. Despite their wide use in OLEDs, 44 ion capture, 47 and cancer therapy, 48 star-shaped Pt(II) complexes remain underexplored for OPL applications.

Based on these considerations, we designed a series of starshaped trinuclear Pt(II) complexes (Pt-1a-Pt-2c) featuring phenyl and triazine cores to enhance the OPL performance of alkylphosphine Pt(II) complexes (Scheme 1). 1,3,5-Triazine, a strong electron acceptor (ionization potential of 11.67 eV) with an excellent photothermal stability, is widely used in starshaped π -conjugated systems. ^{42,49} The incorporation of trinuclear Pt centers markedly enhances the ESA. By modulating the electronic interactions between the cores and the ethynyl ligands (carbazole, fluorene, and naphthalimide), the groundand excited-state properties of Pt-1a-Pt-2c were precisely tuned. Additionally, bulky alkyl chains suppressed the aggregation and improved the solubility of these complexes. As expected, Pt-1a-Pt-2c exhibited extended triplet state lifetimes and enhanced ESA, with their optical transparency and OPL performance optimized by core-ethynyl ligand interactions. In particular, Pt-2b showed the strongest OPL responses at 532 nm while maintaining high transparency. Moreover, the flexible Pt-2b@PDMS films displayed remarkable OPL performance, making them ideal candidates for practical OPL applications. This study reveals the essential roles of metal centers and ligand engineering in tuning the OPL properties of Pt(II) complexes and provides a new strategy for designing advanced OPL materials.

Results and discussion

Synthesis and characterization

The synthetic routes for Pt-1a-Pt-2c are shown in Scheme 2, with detailed experimental procedures provided in the ESI.† Briefly, compounds 1a-1c were reacted with trans-[Pt (PBu₃)₂Cl₂] via the Sonogashira cross-coupling reactions to afford precursors Pt-Cl-a-Pt-Cl-c. In the presence of TBAF, Et₃N



Pt-1a: X = C, Ar = a; **Pt-2a:** X = N, Ar = a**Pt-1b:** X = C, Ar = b; **Pt-2b:** X = N, Ar = b

Pt-1c: X = C, Ar = c; **Pt-2c:** X = N, Ar = c

Star-shaped trinuclear Pt(II) complexes

- ✓ Maintained high optical transparency
- ✓ Extended triplet state lifetimes
- ✓ Enhanced excited-state absorption
- ✓ Excellent optical power limiting performance

Scheme 1 Molecular structures of star-shaped Pt(II) complexes Pt-1a-Pt-2c.

$$Ar = \frac{\text{trans-Pt}(PBu_3)_2Cl_2}{CuI, Et_3N} Ar = \frac{PBu_3}{Pt-Cl} Ar = \frac{PBu_3}{Pt-Cl} Ar = \frac{Pt-1a-Pt-1c}{Pt-1a-Pt-1c} Ar = \frac{Pt-1a-Pt-1c}{Pt-1a-Pt-2c} Ar = \frac{Pt-1a-Pt-1c}{Pt-1a-Pt-2c} Ar = \frac{Pt-1a-Pt-1c}{Pt-1a-Pt-2c} Ar = \frac{Pt-2a-Pt-2c}{Pt-2a-Pt-2c}$$

Scheme 2 Synthetic routes for Pt-1a-Pt-2c.

and CuI, the trimethylsilyl (TMS)-protected compounds 2 or 3 underwent deprotection, followed by in situ base-catalyzed dehydrohalogenation reactions with Pt-Cl-a-Pt-Cl-c to give Pt-1a-Pt-2c in high yields (73%-85%).

Pt-1a-Pt-2c were characterized using ¹H, ¹³C, and ³¹P NMR spectroscopies and MALDI-TOF-MS (see ESI†). In the ³¹P NMR spectra, all complexes displayed sharp singlet signals flanked by two ¹⁹⁵Pt satellites, with ${}^{1}J_{\text{Pt-P}}$ of ~2350 Hz, indicating a trans-P-Pt-P configuration. These data confirmed the successful synthesis of Pt-1a-Pt-2c. They were highly soluble in common organic solvents (e.g., toluene and THF) and exhibited excellent stability (Fig. S25†), with no sensitivity to light or oxygen. TGA curves indicated that the decomposition temperatures ($T_{\rm d}$) exceeded 306 °C, demonstrating their high thermal stability (Fig. S26†).

X-Ray crystal structures

The molecular structures of Pt(II) complexes were determined by single-crystal X-ray diffraction. Single crystals of Pt-1b, Pt-2b, Pt-1c, and Pt-2c were grown by layering ethanol onto a concentrated CH₂Cl₂ solution. Despite multiple attempts, suitable crystals for Pt-1a and Pt-2a could not be obtained. The crystallographic data are summarized in Tables S1 and S2,† with selected bond lengths and bond angles listed in Tables S3-S6.† ORTEP diagrams and packing models are shown in Fig. S27-S30.†

All four complexes crystallized in the triclinic $P\bar{1}$ space group. The asymmetric units of Pt-1b, Pt-2b, and Pt-1c each contain one molecule, while that of Pt-2c contains two. Fig. 1a-d illustrate that the Pt(II) complexes exhibit the anticipated star-shaped structure with each Pt center adopting a slightly distorted square-planar geometry, where the two PBu₃ groups and ethynyl ligands are in a trans-arrangement. The C-Pt-P bond angles range from 85.2(3)° to 95.7(4)°, which alleviates steric hindrance between the PBu₃ groups. The Pt-P and Pt-C bond lengths (2.25(4)-2.41(7) Å and 1.77(12)-2.07(11) Å, respectively) are consistent with those of reported alkylphosphine Pt(II) complexes. 35,41,50

Significant differences are observed in dihedral angles between the cores and ethynyl ligands among the Pt(II) complexes. The dihedral angles between the fluorene units and the core are 22.43°, 24.84°, and 80.78° for Pt-1b, and 8.41°, 27.02°, and 58.75° for Pt-2b. In contrast, Pt-1c and Pt-2c exhibit obviously smaller dihedral angles between the naphthalimide units and the core, suggesting better coplanarity. In the crystal structures, Pt-1b and Pt-2b are primarily stabilized by C-H $\cdots\pi$ interactions (2.92–3.72 Å, Fig. 1e and f). Notably, C-H...Pt interactions (2.75 Å) are also observed in the Pt-2b dimer. For the trimers of Pt-1c and Pt-2c, multiple weak interactions are present, including C-H··· π (2.67-3.61 Å), C-H···N (3.09 and 2.62 Å), and C-H···O interactions (2.72 and 2.57 Å), as shown in Fig. 1g and h. A summary of these interactions is provided in Table S7.† The PBu3 groups extend the intermolecular contact distances, resulting in the absence of Pt···Pt interactions. Nevertheless, sliding π - π stacking are observed between the naphthalimide units in Pt-1c and Pt-2c, with centroid-to-centroid distances of 3.53 and 3.61 Å, respectively. These results suggest that the fluorene units in Pt-1b and Pt-**2b** introduce significant distortion, effectively suppressing π - π stacking and promoting homogeneous dispersion within polymer matrices.

Photophysical properties

Absorption spectra. The UV-vis absorption spectra of Pt-1a-Pt-2c were recorded in CH₂Cl₂, with the photophysical parameters summarized in Table 1. As illustrated in Fig. 2a, all the complexes showed intense absorption bands, attributed to Pt center-disturbed ${}^{1}\pi$ - π^* transitions of ethynyl ligands. **Pt-1a** and

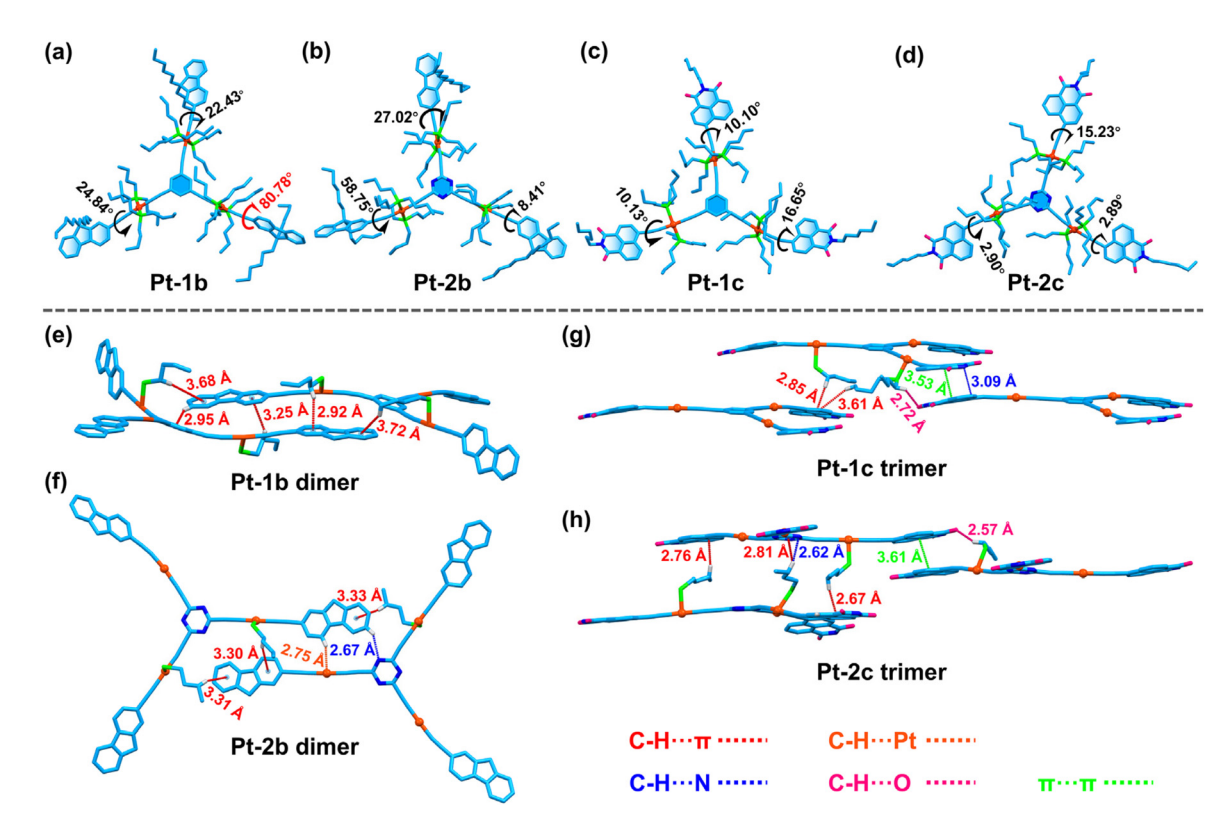


Fig. 1 (a-d) Single-crystal structures of Pt-1b, Pt-2b, Pt-1c, and Pt-2c (Color codes: cyan-green = C, light gray = H, blue = N, pink = O, green = P, and orange = Pt). (e-h) Crystal packing modes of Pt-1b, Pt-2b, Pt-1c, and Pt-2c. Partial H atoms, C_6H_{13} chains, and PBu₃ groups are omitted for clarity.

Table 1 Photophysical parameters for Pt-1a-Pt-2c

Research Article

Complexes	$\lambda_{ m abs}^{a}/ m nm$	$\lambda_{\mathrm{em}}/\mathrm{nm} \left(\tau_{\mathrm{em}}/\mu \mathrm{s} \right)^b$	$\lambda_{\rm em}/{\rm nm} \left(au_{\rm em}/\mu {\rm s} \right)^c$	${m \Phi_{ m P}}^d/\%_0$	$\lambda_{\mathrm{T1-T}n}/\mathrm{nm}\left(au_{\mathrm{T}}/\mathrm{\mu s}\right)^{e}$	$\lambda_{\mathrm{cut\text{-}off}}/\mathrm{nm}$
Pt-1a	293, 310, 345	401, 462	460 (78.61)	_	_	388
Pt-2a	95, 309, 324, 356	401, 452	453 (37.59)	_	_	405
Pt-1b	297, 358	380, 507 (0.93)	507 (202.04)	15.31	560 (0.96)	383
Pt-2b	299, 352	389, 506 (0.50)	505 (211.40)	18.28	530 (0.52)	395
Pt-1c	284, 320, 349, 435	512, 639 (1.98)	483, 634 (368.01)	6.77	628 (2.05)	498
Pt-2c	298, 427	491	463, 629 (435.75)	_	640 (1.59)	480

 $[^]a$ UV-vis absorption band maxima in CH₂Cl₂. b Emission band maxima and phosphorescence lifetimes measured in deaerated CH₂Cl₂. c Emission band maxima and decay lifetimes of T₁ state recorded in 2-Me THF at 77 K. d Absolute phosphorescence quantum yields measured in deaerated CH₂Cl₂ using an integrating sphere. e ns-TA band maxima or triplet state lifetimes in deaerated toluene.

Pt-2a displayed two main absorption peaks between 280-390 nm, along with a moderate band at ca. 310 nm, likely from metal-centered (MC) transitions.⁵¹ Pt-1b and Pt-2b exhibited similar absorption features below 400 nm (280-305 nm and 305–380 nm), with maximum absorption wavelengths (λ_{abs}) of 358 nm and 352 nm, respectively. However, the cut-off wavelength ($\lambda_{\text{cut-off}}$) of **Pt-2b** was red-shifted by 12 nm. Meanwhile, the d_{π} - π orbital mixing led to red-shifted absorption compared with their precursors Pt-Cl-a-Pt-Cl-c (Fig. S31†). Nevertheless, the $\lambda_{\text{cut-off}}$ of **Pt-1a**, **Pt-2a**, **Pt-1b**, and **Pt-2b** remained below 405 nm, ensuring high optical transparency.

In contrast, Pt-1c and Pt-2c, bearing naphthalimide units with strong ${}^{1}\pi$ - π * transition absorptions near 430 nm, exhibited a $\lambda_{\text{cut-off}}$ extending beyond 480 nm, resulting in reduced transparency. Furthermore, the absorption spectra in different solvents revealed that the absorption peaks of Pt-2a, Pt-2b, and Pt-1c broadened more noticeably in polar solvents (Fig. S32†), indicating stronger intramolecular charge transfer (ICT) effects than Pt-1a, Pt-1b, and Pt-2c. These enhanced ICT characteristics are expected to improve their OPL responses.

Emission spectra. The emission spectra of Pt-1a-Pt-2c in deaerated CH₂Cl₂ are shown in Fig. 2b. Except for **Pt-2c**, all the complexes exhibited dual emission properties at room temperature. The short-wavelength bands with lifetimes <2 ns were assigned to the lowest singlet state (S₁) fluorescence.⁵² The long-wavelength band, featuring well-resolved vibrational

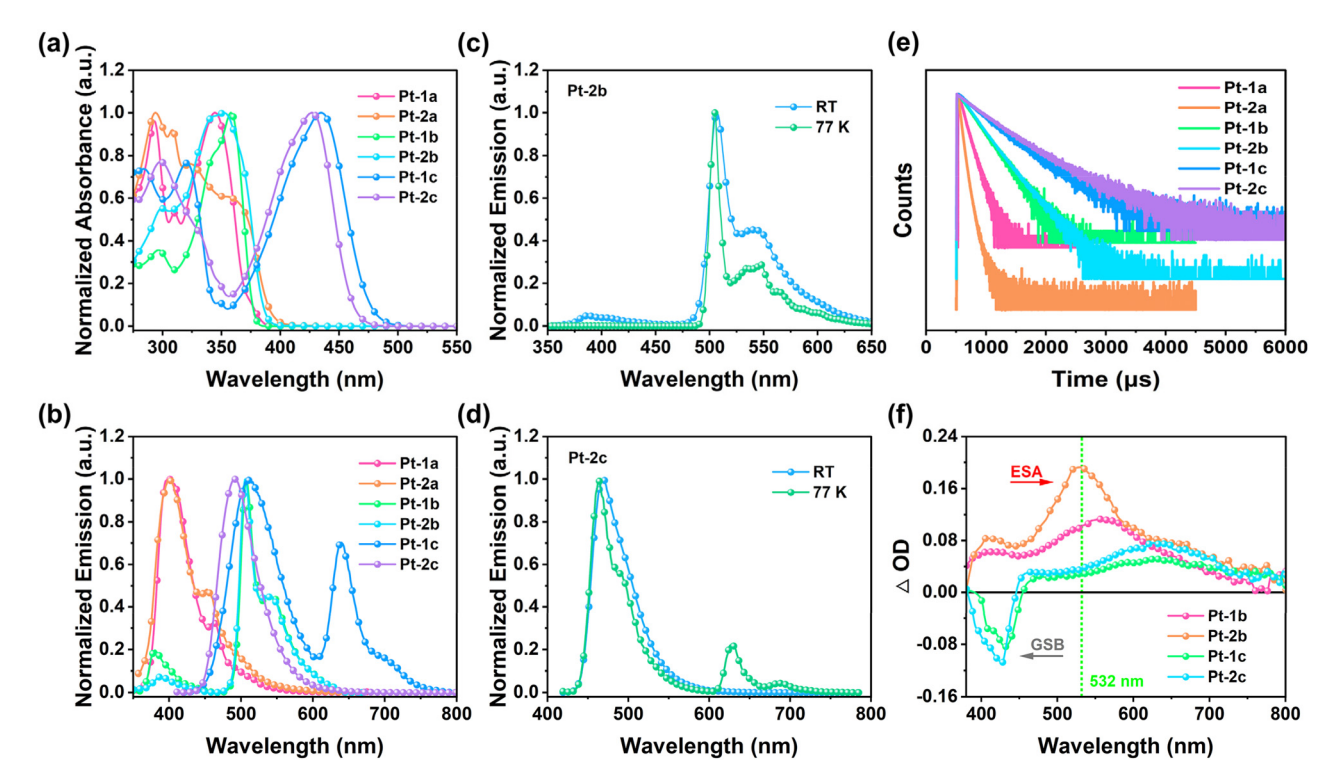


Fig. 2 (a) UV-vis absorption spectra of Pt-1a-Pt-2c in CH₂Cl₂ and (b) emission spectra of Pt-1a-Pt-2c in deaerated CH₂Cl₂ ($c = 1.0 \times 10^{-5}$ mol L⁻¹, r.t.). (c and d) Normalized emission spectra of Pt-2b and Pt-2c in 2-Me THF at r.t. and 77 K, respectively. (e) Emission lifetimes of the T₁ state for Pt-1a-Pt-2c at 77 K. (f) ns-TA spectra of Pt-1b, Pt-2b, Pt-1c, and Pt-2c at zero delay in deaerated toluene (λ_{ex} = 355 nm).

structures, microsecond-scale lifetimes and large Stokes shifts (>100 nm), corresponded to the lowest triplet state (T1) phosphorescence.

The ethynyl ligands successfully influenced the emission properties. For Pt-1a and Pt-2a, phosphorescence appeared as weak shoulders beside fluorescence, while for Pt-1b and Pt-2b phosphorescence was the predominant emission. Pt-2c showed only cyan fluorescence with $\lambda_{\rm em}$ = 491 nm, which was blue-shifted by 20 nm compared with Pt-1c, with a higher fluorescence quantum yield ($\Phi_{\rm F}$ = 5.40%) than the others ($\Phi_{\rm F}$ < 0.05%). The low $\Phi_{\rm F}$ values were attributed to the heavy-atom effect of Pt centers, which enhanced the SOC effect and facilitated ISC from the S₁ state to T₁ state. The absolute phosphorescence quantum yields (Φ_P) for Pt-1b, Pt-2b, and Pt-1c were 15.31%, 18.28%, and 6.77%, respectively (Table 1). Notably, the incorporation of fluorene units enhanced the d_{π} - π orbital coupling, increasing the T1 state populations. Pt-2b showed the highest Φ_P , which could improve the OPL performance via the RSA mechanism.

The fluorescence peaks of Pt-1a-Pt-2c exhibited red-shifts with increasing solvent polarity, suggesting that the S₁ state originated from the mixed ${}^{1}\pi$ - π */ ${}^{1}ICT$ transitions. In contrast, the phosphorescence bands, which were attributed to the predominant ${}^{3}\pi$ - π * transitions, were almost unaffected by solvent polarity (Fig. S33†). These assignments were also supported by theoretical calculations. To further explore the T₁ emissive state properties, low-temperature emission spectra were

recorded (Fig. 2c, d, and S34†). At 77 K, the long-wavelength bands intensified, and their lifetimes were greatly extended (Fig. 2e and Table 1), confirming their phosphorescent origin. However, Pt-1c and Pt-2c still displayed intense fluorescence, suggesting lower T₁ state populations despite their long phosphorescence lifetimes. 41,46

Nanosecond transient absorption spectra. The triplet state properties of Pt-1a-Pt-2c were investigated using ns-TA spectroscopy. Except for the weak TA signals of Pt-1a and Pt-2a, the TA spectra at zero delay and time-resolved TA profiles of the Pt (II) complexes in deaerated toluene are presented in Fig. 2f and Fig. S35.† These complexes exhibited broad and intense ESA bands in the visible to NIR region (380-800 nm for Pt-1b and Pt-2b and 450-800 nm for Pt-1c and Pt-2c), which were stronger than their GSA, indicating the potential for RSA effects. Pt-1c and Pt-2c displayed distinct bleaching bands in the range of 380-450 nm, which were consistent with the GSA (Fig. 2a), confirming that their excited-states are localized on the naphthalimide units. Therefore, the observed triplet states predominantly originated from the ligand-centered $^3\pi$ - π * transitions.53

Fitting the decay curves of the TA signals yielded the triplet state lifetimes (τ_T) for Pt-1b, Pt-2b, Pt-1c, and Pt-2c as 0.96, 0.52, 2.05, and 1.59 µs, respectively (Fig. S36†), indicating their characteristic as long-lived RSA materials. Compared with the precursors (Pt-Cl-b and Pt-Cl-c), they showed significantly enhanced ESA signals and 3-6 times longer triplet lifetimes (Fig. S37†), highlighting the great potential of star-shaped Pt (II) complexes in optimizing the triplet state properties. Although incorporation of the triazine core slightly shortened the triplet state lifetimes of Pt-2b and Pt-2c, it improved their ESA intensity, facilitating the RSA effect. Specifically, Pt-2b showed the strongest ESA across the entire TA spectra, indicating its superior triplet state characteristics and promising OPL responses.

Theoretical calculations

Research Article

Molecular orbital analysis. To understand the observed photophysical phenomena, DFT and TD-DFT calculations were performed to analyze the frontier molecular orbitals (FMOs) of Pt-1a-Pt-2c (Fig. 3a and S38-S43†). The contributions of each fragment to the FMOs are listed in Tables S8-S13,† and the excited-state parameters for the S₁ and T₁ states are summarized in Table 2. As illustrated in Fig. 3a, after introducing triazine core, the LUMO (L) levels of Pt-2a and Pt-2b are greatly reduced compared with Pt-1a and Pt-1b, with the energy gaps (E_{σ}) decreasing by 0.47 and 0.35 eV, respectively. In contrast, the triazine of Pt-2c, lowers the HOMO(H) level by 0.20 eV relative to Pt-1c, increasing E_g to 3.35 eV and resulting in a 40 nm blue-shift in λ_{abs} .

Upon photoexcitation, Pt-1a-Pt-2c exhibit intraligand $^{1}\pi$ - π * transitions, accompanied by varying degrees of ¹ICT effects. Specifically, the H and H-1 of Pt-1a and Pt-1b were delocalized over the entire molecule, while the L and L+1 were mainly localized on the carbazole or fluorene units, exhibiting predominantly ${}^{1}\pi$ - π * transitions with minor ${}^{1}MLCT/{}^{1}LLCT$ features. In Pt-2a, Pt-2b, and Pt-1c, the H and H-1 were mainly localized on the carbazole, fluorene, or phenyl, while the L and L+1 were distributed on the triazine core or naphthalimide units, indicating pronounced ¹LLCT transitions (e.g., carbazole or fluorene \rightarrow triazine, phenyl \rightarrow naphthalimide). For **Pt-2c**, the electron density was entirely localized on the naphthalimide units, exhibiting predominately ${}^{1}\pi$ - π * transitions. Additionally, the Pt atoms contribute differently to their FMOs. For Pt-1a, Pt-1c, and Pt-2c, the Pt atoms contribute 10.50-25.80% to the H and H-1, while their contribution to the L and L+1 is negligible, suggesting some ${}^{1}MLCT$ (Pt \rightarrow ethynyl ligands) features. In contrast, Pt atoms contribute more (>3.07%) to the L and L+1 of Pt-1b and Pt-2b, imparting slight ligand-to-metal charge transfer (¹LMCT) transitions, which are beneficial for enhancing their OPL responses.41

Natural transition orbital analysis. To investigate the origin of phosphorescent emission in Pt-1a-Pt-2c,45 natural transition orbitals (NTOs) were calculated based on the optimized T_1 state geometries. As presented in Fig. 3b, the hole \rightarrow particle transitions contributed over 97.2% to the T₁ state. The ethynyl ligands accounted for more than 82.17% to both hole and particle, while the contribution from Pt atoms ranged from 2.29% to 11.14%, with a higher contribution to the hole

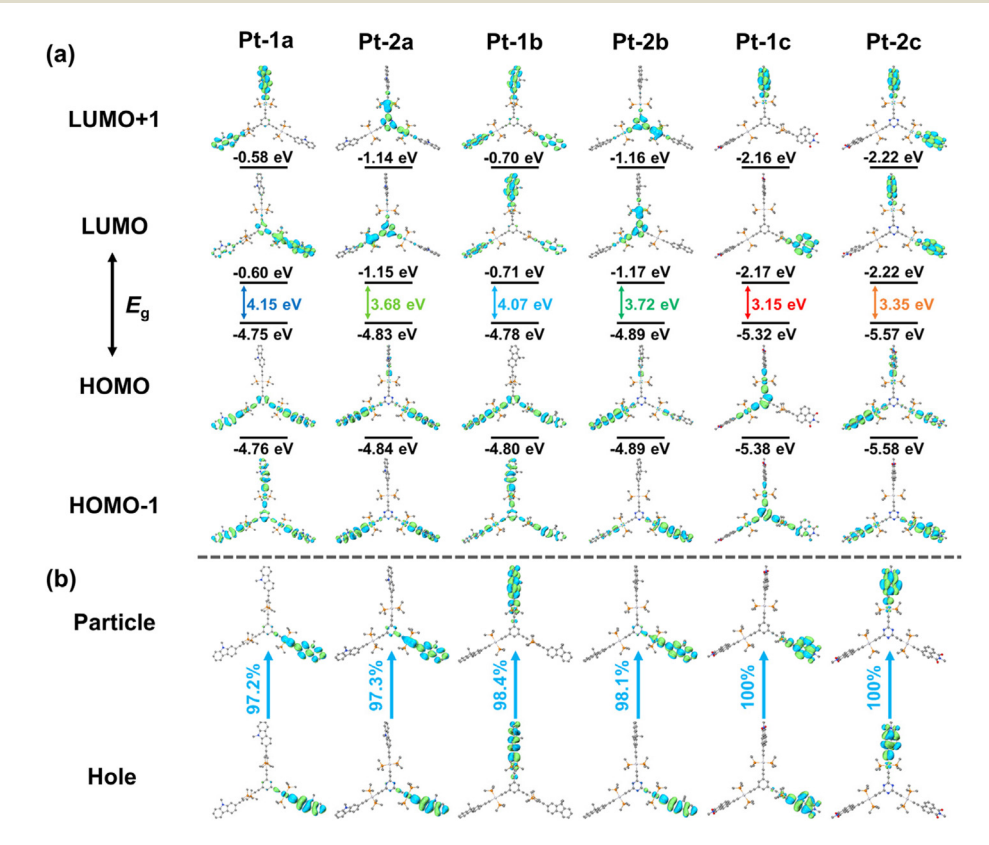


Fig. 3 (a) Contour plots of HOMO, HOMO-1, LUMO, and LUMO+1 for Pt-1a-Pt-2c based on optimized S₀ geometries. (b) Distribution patterns of NTOs for $S_0 \rightarrow T_1$ excitation of Pt-1a-Pt-2c based on optimized T_1 geometries.

Table 2 Excitation energies (eV), wavelengths (nm), oscillator strengths (f), and dominant contributing configurations of the S₁ and T₁ states for Pt-1a–Pt-2c based on their optimized S₀ geometries

Complexes	State	Excitation energy/eV (Wavelength/nm)	f	Orbital contribution (>10%)	Assignment
Pt-1a	S ₁	3.60 (344)	0.440	$H \to L (38\%), H \to L+3 (11\%)$	¹ IL/ ¹ MLCT
	T_1	2.67 (463)	0.000	$H-3 \rightarrow L+3 (15\%), H-4 \rightarrow L+4 (13\%)$	3IL/3MLCT/3LLCT
Pt-2a	S_1	3.23 (383)	0.088	$H \to L (68\%), H-2 \to L (17\%)$	1 IL/ 1 LLCT
	T_1	2.69 (460)	0.000	$H \rightarrow L+2 (57\%)$	³ IL/ ³ MLCT
Pt-1b	S_1	3.58 (346)	0.963	$H \to L+2(18\%), H \to L+3 (25\%)$	¹ IL/ ¹ LLCT/ ¹ LMCT
	T_1	2.60 (476)	0.000	$H-1 \rightarrow L (62\%)$	³ IL/ ³ LLCT
Pt-2b	S_1	3.26 (380)	0.0366	$H \rightarrow L (81\%)$	¹ IL/ ¹ LLCT/ ¹ LMCT
	T_1	2.61 (475)	0.000	$H \rightarrow L+2 (62\%)$	³ IL/ ³ MLCT
Pt-1c	S_1	2.77 (447)	0.001	$H \to L (68\%), H-1 \to L (19\%)$	¹ IL/ ¹ MLCT/ ¹ LLCT
	T_1	1.97 (629)	0.000	$H-4 \rightarrow L (57\%), H-1 \rightarrow L (21\%)$	3IL/3MLCT/3LLCT
Pt-2c	S_1	3.04 (407)	1.138	$H \rightarrow L (67\%)$	¹ IL/ ¹ MLCT
	T_1	1.98 (626)	0.000	$H \rightarrow L (82\%)$	³ IL/ ³ MLCT

(Table S14†). These results indicated that the T_1 state of **Pt-1a-Pt-2c** primarily originated from ${}^3\pi^-\pi^*$ transitions, with a minor 3MLCT character, consistent with the experimental observations. The contribution of Pt atoms to both the hole and particle in **Pt-1c** and **Pt-2c** was lower than the other complexes, indicating a weaker $d_\pi^-\pi$ coupling and consequently inhibiting the ISC process. The intense fluorescence observed for **Pt-1c** and **Pt-2c** at 77 K further supported this conclusion.

Nonlinear optical properties

Third-order nonlinear optical properties. Based on the broad and intense ESA signals observed in the ns-TA spectra, the NLO properties were evaluated using an open-aperture Z-scan technique (Fig. 4a). Detailed experimental procedures and data fitting for the Z-scan are included in the ESI.† Under 532 nm pulsed laser irradiation (4.0 ns, 100 μ J), the Z-scan curves of Pt-1a–Pt-2c in toluene exhibited obvious RSA characteristics (Fig. 4b and S44†), with the minimum normalized transmittance (T_{\min}) at the focal point (Z = 0) ranging from 0.38 to 0.78, indicating tunable NLO properties. As expected, Pt-2b showed the lowest T_{\min} value of 0.38, demonstrating the best NLO properties.

To quantitatively compare their NLO properties, the effective nonlinear absorption coefficients ($\beta_{\rm eff}$) were extracted by fitting the *Z*-scan data. **Pt-2a** (31.60 cm GW⁻¹), **Pt-2b** (192.15 cm GW⁻¹), and **Pt-1c** (83.52 cm GW⁻¹) showed higher $\beta_{\rm eff}$ values than **Pt-1a** (26.49 cm GW⁻¹), **Pt-1b** (125.33 cm GW⁻¹), and **Pt-2c** (67.45 cm GW⁻¹), which can be attributed to their stronger ICT effects (Fig. 4c). The $\beta_{\rm eff}$ value of **Pt-2b** surpassed those of most alkylphosphine Pt(II) complexes, ^{29,54,55} many cyclometalated Pt(II) complexes and Pt(II)-incorporated copolymers. ⁵⁶ The outstanding NLO response of **Pt-2b** originated from the strong SOC-facilitated ISC, along with ICT effects, which synergistically enhanced its ESA.

Optical power limiting performance. OPL is a key application in the NLO field. At low incident fluence, Pt-1a-Pt-2c showed a linear input-output relationship with high transmittance. As fluence increased, the output fluence gradually decreased and tended to saturate, displaying a typical OPL behavior (Fig. 4d). The OPL performance followed the trend of

Pt-2b > Pt-1b > Pt-1c > Pt-2c > Pt-2a > Pt-1a, which was consistent with the *Z*-scan results. Compared with electron-donating carbazole and electron-withdrawing naphthalimide units, the weakly donating fluorene units in Pt-1b and Pt-2b enhanced their OPL performance. As shown in Fig. 4e, the optical limiting thresholds (F_{OL} , defined as the incident fluence at 50% linear transmittance) for Pt-1b and Pt-2b were 0.88 and 0.71 J cm⁻², respectively. Owing to the strong ESA, they exhibited markedly enhanced NLO and OPL performances compared with their precursor Pt-Cl-b (Fig. 4f and g).

The OPL mechanism is illustrated in the Jablonski diagram (Fig. 4h). Under 532 nm excitation, the molecule underwent rapid ISC from the S_1 state to the T_1 state. The long triplet state lifetimes enabled the accumulation of T_1 state populations and promoted the subsequent T_1 – T_n absorption (ESA), thereby inducing OPL effects. Therefore, the OPL performance of **Pt-1a–Pt-2c** closely correlated with their ESA intensity. **Pt-2b** exhibited the strongest ESA at 532 nm, thus achieving the best OPL performance. Although **Pt-1c** and **Pt-2c** showed lower T_1 state populations, their long triplet state lifetimes (1.59 and 2.05 μ s) and moderate ESA intensities still provided considerable OPL responses. In contrast, the undetectable ESA signals of **Pt-1a** and **Pt-2a** in the TA spectra accounted for their weak OPL activities.

Solid-state optical limiter

Solid-state optical limiters offer many advantages for practical applications. Various OPL materials have been successfully integrated into polymer matrices, such as poly(methyl methacrylate) (PMMA), methyltriethoxysilane (MTES), and PDMS, to fabricate doped films or gel glasses. To Given the high transparency and superior OPL performance of Pt-2b, it was incorporated into PDMS to fabricate flexible and transparent Pt-2b@PDMS films (Fig. 5a). As a chemically inert material with excellent optical transparency, thermal stability, and flexibility, PDMS ensured uniform dispersion of Pt-2b without any chemical interactions. Pt-2b@PDMS films with various concentrations (0-1.00 wt%) displayed uniform color and smooth, defect-free surfaces that are suitable for optical measurements (Fig. 5b). SEM-EDS analysis confirmed the homogeneous dis-

Research Article

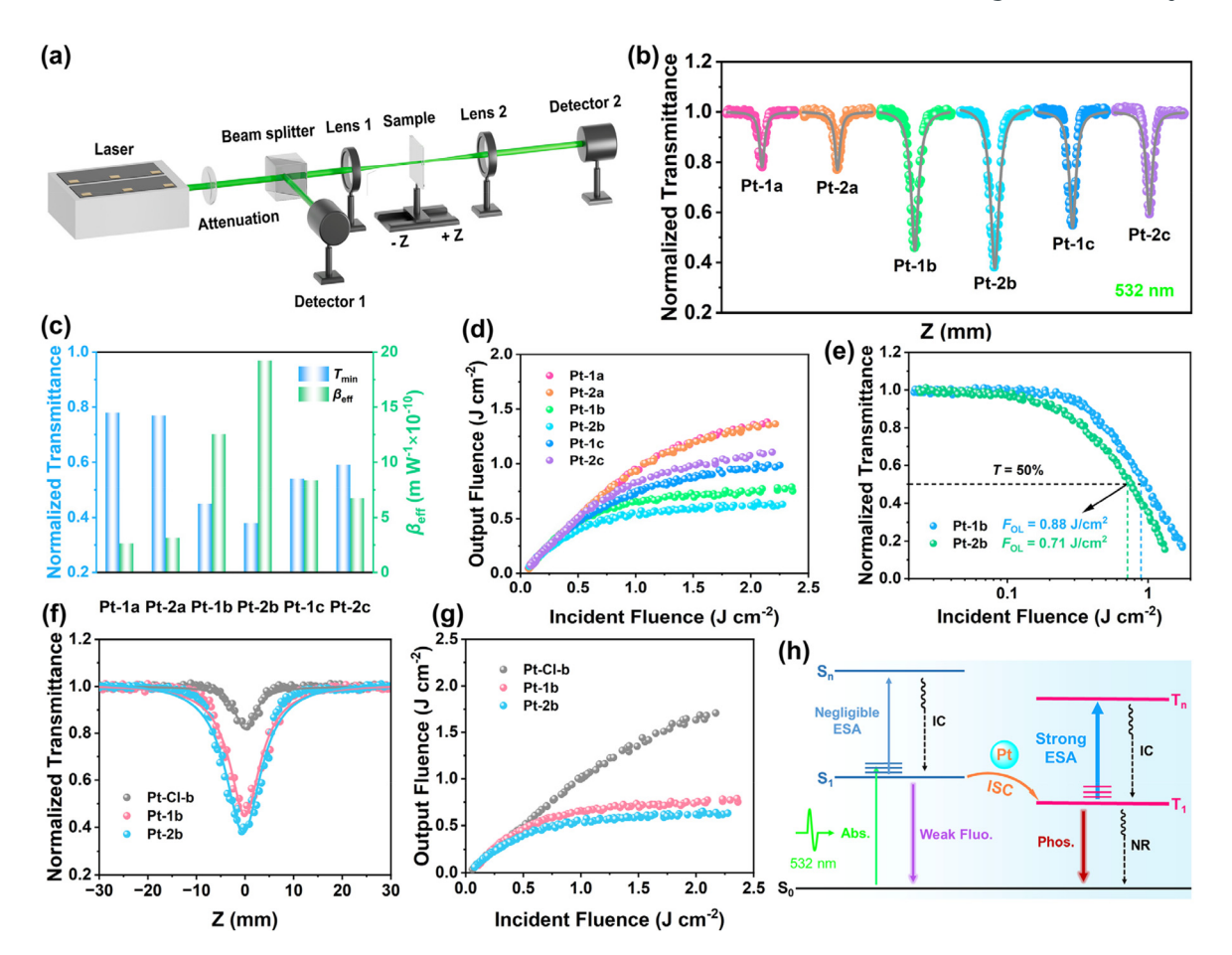


Fig. 4 (a) Schematic of the Z-scan setup. (b) Open-aperture Z-scan (points) and theoretical fit (solid lines) curves of Pt-1a-Pt-2c in toluene (c = 1.0 mM) at 532 nm. (c) Comparison of the T_{min} and β_{eff} value for Pt-1a-Pt-2c. (d) Output fluence versus input fluence curves for Pt-1a-Pt-2c. (e) Nonlinear transmittance versus input fluence curves of Pt-1b and Pt-2b. (f) Open-aperture Z-scan curves and (g) output fluence versus input fluence curves for Pt-Cl-b, Pt-1b, and Pt-2b. (h) Jablonski diagram for Pt-1a-Pt-2c based on the RSA mechanism.

tribution of Pt-2b within the PDMS matrix (Fig. S45†). Under visible light, the films maintained high optical transparency, clearly revealing the underlying patterns. The pristine PDMS film displayed a linear transmittance (T_0) above 90% across the visible spectrum. With increasing Pt-2b content, T_0 gradually decreased; for Pt-2b@PDMS-1.00 wt%, the T_0 value at 532 nm remained 67%, meeting the practical OPL requirements (Fig. 5c). Even at an increased concentration of 5.00 wt%, Pt-2b remained uniformly dispersed in the PDMS matrix (Fig. S46†) owing to its twisted molecular structure and lack of π - π stacking, which effectively prevented aggregation, along with bulky alkyl chains that enhanced its compatibility with PDMS.

Under pulsed laser irradiation at 100 µJ, the pristine PDMS film exhibited no detectable NLO response (Fig. S47†), confirming that the polymer matrix has negligible influence on the NLO properties. As shown in Fig. 5d and e, the NLO and OPL responses of Pt-2b@PDMS increased with Pt-2b concentration. The T_{\min} dropped from 0.46 (0.05 wt%) to 0.11 (1.00 wt%), while the $\beta_{\rm eff}$ value increased accordingly, indicating that the NLO performance was concentration-dependent. Table S15† summarizes the linear and NLO parameters of Pt-2b@PDMS films at various

concentrations. At 1.00 wt%, $\beta_{\rm eff}$ reached 965.83 cm GW⁻¹, rivaling or surpassing the $eta_{
m eff}$ values of the state-of-the-art NLO materials (Table 3). 14,61,62 Besides, Pt-2b@PDMS-1.00 wt% demonstrated excellent OPL performance, with an optical limiting onset threshold (F_{ON} , defined as the incident fluence at 95% linear transmittance) and $F_{\rm OL}$ value of only 0.037 and 0.26 J cm⁻², respectively (Fig. 5f). As illustrated in Fig. 5g and Table 3, its performance surpassed those of many representative solid-state OPL limiters, including TTF-Pt(bzimb),9 metal clusters (V9Mo1 and InOC-19),^{22,63} Al molecular rings (AlOC-93 and AlOC-135),^{53,54} MOF (ZnTPy-1),14 COF (CuPc-PI-COF-1),64 and composites ((MX@NCS)₄ and MoS₂-PAN).^{65,66}

Compared with the solution state, Pt-2b@PDMS exhibited significantly enhanced OPL performance, with a nearly 5 times higher β_{eff} value (Fig. S48†). This enhancement can be attributed to the suppressed molecular distortion and reduced ³O₂induced T₁ state quenching in the solid matrix, thereby increasing T₁ state populations. To highlight the advantages of Pt-2b, a comparison with C₆₀@PDMS showed that Pt-2b@PDMS not only displayed a stronger OPL performance but also a higher transparency (Fig. S49 and S50†). These findings

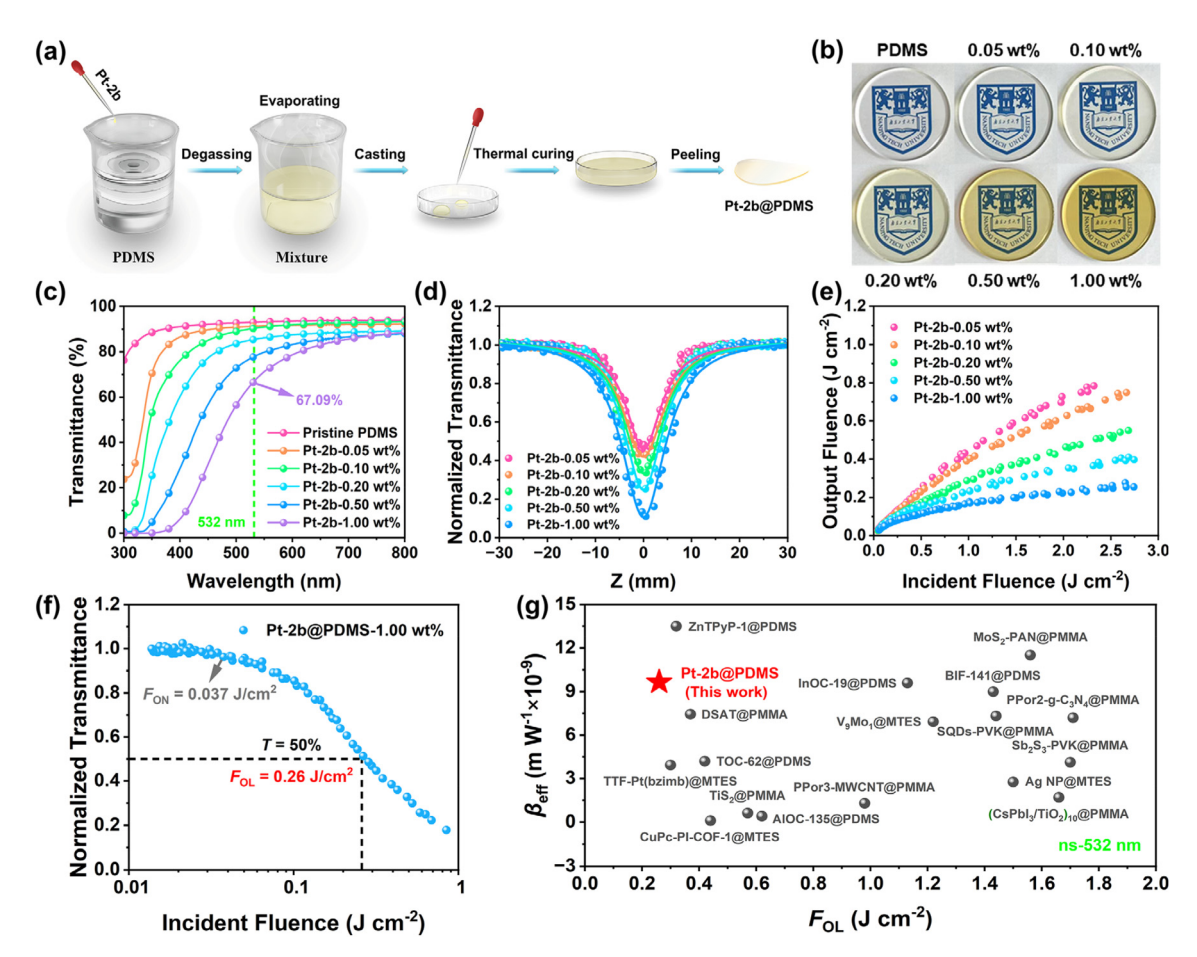


Fig. 5 (a) Schematic of the preparation process for Pt-2b@PDMS films. (b) Optical photographs of Pt-2b@PDMS films at various concentrations (diameter: 40 mm; thickness; 2 mm), (c) Linear transmittance spectra of Pt-2b@PDMS films, (d) Open-aperture Z-scan curves and (e) output fluence versus input fluence curves for Pt-2b@PDMS films at various concentrations at 532 nm. (f) Nonlinear transmittance versus input fluence curve of Pt-**2b@PDMS-1.00 wt%**. (g) Comparison of the β_{eff} and F_{Ol} values of **Pt-2b@PDMS-1.00 wt%** with those of representative solid-state optical limiters.

Table 3 Comparison of the third-order NLO properties of representative solid-state optical limiters at 532 nm

Sample	Parameters ^a	L^b (mm)	c ^c (wt %)	T_0^{d} (%)	β^e (cm GW ⁻¹)	$F_{ m OL}^f$ (J cm ⁻²)	Ref.
Pt-2b@PDMS	4 ns, 10 Hz	2	1.00	67	965.83	0.26	This work
AlOC-135@PDMS	8.5 ns, 10 Hz	_	_	51	41	0.62	Inorg. Chem. Front., 2024, 11 , 462–469 ⁶⁷
AlOC-93@PDMS	8.5 ns, 10 Hz	2	_	38	71.80	0.12	Aggregate, 2023, 4, e264 ⁶⁸
ZnTPyP-1@PDMS	5 ns, 5 Hz	2	0.25	62	1350	0.32	J. Am. Chem. Soc., 2021, 143, 17162–17169 ¹⁴
CuPc-PI-COF-1@MTES	8 ns, 10 Hz	_	_	_	10.72	0.44	Adv. Funct. Mater., 2024, 34 , 2404289 ⁶⁴
V ₉ Mo ₁ @MTES	10 ns, 10 Hz	_	1.00	<40	691.79	1.22	Inorg. Chem. Front., 2022, 9 , 4413–4424 ⁶³
TTF-Pt(bzimb)@MTES	8 ns, 10 Hz	_	3.33	41	393	0.30	J. Mater. Chem. C, 2018, 6, 8495-8501 ⁹
(MX@NCS) ₄ /PMMA	6 ns, 1 Hz	1	4.00	_	387	0.21	Small, 2025, 2411146 ⁶⁵
DAST@PMMA	6 ns, 2 Hz	0.1	0.125	85	744	0.37	ACS Appl. Mater. Interfaces, 2022, 14 , 33787–33796 ⁵⁷
MoS ₂ -PAN@PMMA	8 ns, 2 Hz	_	_	~64	1151.01	1.56	J. Mater. Chem. C, 2017, 5, 11920-11926 ⁶⁶

^a Laser pulse width and repetition rate of 532 nm laser. ^b Thickness of the film. ^c Dopant concentration. ^d Linear transmittance at 532 nm. ^e Nonlinear absorption coefficient. ^fOptical limiting threshold.

suggest the potential of Pt-2b@PDMS films for laser protection applications.

Stability of Pt-2b@PDMS films

Benefiting from its low Young's modulus, Pt-2b@PDMS-1.00 wt% retained its original shape after 100 cycles of stretching, twisting,

and folding (Fig. 6a). The stress-strain curves showed that Pt-2b induced a negligible effect on the mechanical properties of PDMS, with the tensile strength increasing slightly from 8.09 to 8.11 MPa and the modulus from 7.50 to 7.60 MPa (Fig. 6b). TGA analysis revealed that both pristine PDMS and Pt-**2b@PDMS-1.00 wt%** exhibited $T_{\rm d}$ values above 391 °C, confirm-

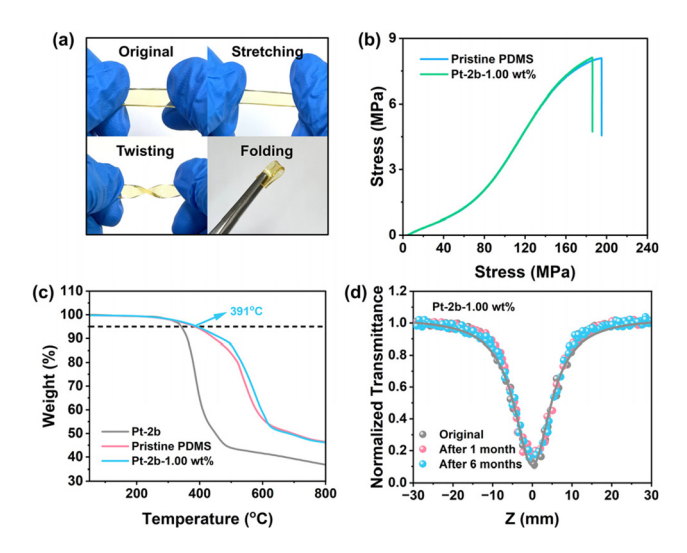


Fig. 6 (a) Illustration of the mechanical flexibility of Pt-2b@PDMS-1.00 wt%. (b) Stress—strain curves of pristine PDMS and Pt-2b@PDMS-1.00 wt%. (c) TGA curves of Pt-2b, pristine PDMS, and Pt-2b@PDMS-1.00 wt%. (d) Open-aperture Z-scan curves for Pt-2b@PDMS-1.00 wt% after storage for various durations.

ing their excellent thermal stability (Fig. 6c). Moreover, the NLO responses of the film remained nearly unchanged over time, indicating good durability (Fig. 6d). The combination of strong OPL performance, high transparency, and exceptional stability makes **Pt-2b@PDMS** a promising candidate for OPL devices.

Conclusions

In summary, six star-shaped Pt(II) complexes were synthesized to tune their photophysical properties and enhance their OPL performance. Spectroscopic and theoretical analyses showed that the S_1 states of **Pt-1a-Pt-2c** involved mixed ${}^1\pi - \pi^*/{}^1$ ICT transitions, while the T_1 states were mainly localized ${}^3\pi$ - π * transitions on ethynyl ligands. The incorporation of trinuclear Pt centers extended the triplet state lifetimes and enhanced the ESA, with core-ethynyl ligand electronic effects playing crucial roles in regulating the photophysical properties. Pt-2b exhibited outstanding OPL responses while maintaining excellent transparency, surpassing many representative OPL materials. The corresponding Pt-2b@PDMS-1.00 wt% film exhibited a remarkable OPL performance, featuring a high $\beta_{\rm eff}$ of 965.83 cm GW⁻¹ and a low $F_{\rm OL}$ of 0.26 J cm⁻², demonstrating its potential for practical OPL applications. This work highlights the structure-property relationships in Pt(II) complexes and provides a promising strategy for designing next-generation OPL materials. Future work will explore their broadband OPL properties in the NIR region and further investigate their application in flexible photonic devices.

Author contributions

Lai Hu: methodology, data curation, writing – original draft; Zhiyuan Chen: investigation; Zhi Zhao: data curation; Ruiqi Chen: conceptualization; Senqiang Zhu: conceptualization, writing – review and editing; Rui Liu: funding acquisition, supervision; Hongjun Zhu: funding acquisition, supervision.

Conflicts of interest

There are no conflicts to declare.

Data availability

The data supporting this article have been included as part of the ESI.†

Acknowledgements

The authors greatly acknowledge the National Key R&D Program of China (2023YFA0913600), the Natural Science Foundation of Jiangsu Province (BK20220351) and the Natural Science Foundation of the Jiangsu Higher Education Institutions of China (No. 22KJB150027) for the financial support.

References

- 1 Q. Guo, R. Sekine, L. Ledezma, R. Nehra, D. J. Dean, A. Roy, R. M. Gray, S. Jahani and A. Marandi, Femtojoule Femtosecond All-Optical Switching in Lithium Niobate Nanophotonics, *Nat. Photonics*, 2022, 16, 625–631.
- 2 K. Geng, Y. Sun, Y. Zhao, Z. Shao, Y. Wei, J. Huang, Y. Cui, X. Xu and H. Hou, Giant Enhancement of Optical Nonlinearity by Manipulating Guest Molecular Stacking Modes in Metal-Organic Frameworks, *J. Am. Chem. Soc.*, 2025, 147, 9844–9857.
- 3 Z. Sun, T. Hasan, F. Torrisi, D. Popa, G. Privitera, F. Wang, F. Bonaccorso, D. M. Basko and A. C. Ferrari, Graphene Mode-Locked Ultrafast Laser, ACS Nano, 2010, 4, 803–810.
- 4 D. Dini, M. J. F. Calvete and M. Hanack, Nonlinear Optical Materials for the Smart Filtering of Optical Radiation, *Chem. Rev.*, 2016, 116, 13043–13233.
- 5 X. Feng, Z. Shi, J. Chen, T. Yu, X. Jiang, G. Du, J. Qiu and S. Zhou, All-Inorganic Transparent Composite Materials for Optical Limiting, *Adv. Opt. Mater.*, 2020, **8**, 1902143.
- 6 K. S. Krishna, C. S. S. Sandeep, R. Philip and M. Eswaramoorthy, Mixing Does the Magic: A Rapid Synthesis of High Surface Area Noble Metal Nanosponges Showing Broadband Nonlinear Optical Response, ACS Nano, 2010, 4, 2681–2688.
- 7 Y. Song, J. Sun, X. He, M. Liao, J. Zhao, W. Zeng, S. Zhou and H. Chen, N-Doped Nonalternant Nanoribbons with Excellent Nonlinear Optical Performance, *Angew. Chem., Int. Ed.*, 2023, **62**, e202306418.
- 8 M. O. Senge, M. Fazekas, E. G. A. Notaras, W. J. Blau, M. Zawadzka, O. B. Locos and E. M. Ni, Mhuircheartaigh,

- Nonlinear Optical Properties of Porphyrins, *Adv. Mater.*, 2007, **19**, 2737–2774.
- 9 J. Sun, B. Yuan, X. Hou, C. Yan, X. Sun, Z. Xie, X. Shao and S. Zhou, Broadband Optical Limiting of a Novel Twisted Tetrathiafulvalene Incorporated Donor–Acceptor Material and Its Ormosil Gel Glasses, *J. Mater. Chem. C*, 2018, 6, 8495–8501.
- 10 Z. Liu, J. Sun, C. Yan, Z. Xie, G. Zhang, X. Shao, D. Zhang and S. Zhou, Diketopyrrolopyrrole Based Donor–Acceptor π-Conjugated Copolymers with near-Infrared Absorption for 532 and 1064 nm Nonlinear Optical Materials, *J. Mater. Chem. C*, 2020, 8, 12993–13000.
- 11 S. Hirata, K. Totani, T. Yamashita, C. Adachi and M. Vacha, Large Reverse Saturable Absorption under Weak Continuous Incoherent Light, *Nat. Mater.*, 2014, 13, 938– 946.
- 12 B. Fang, Y. Zhu, L. Hu, Y. Shen, G. Jiang, Q. Zhang, X. Tian, S. Li, H. Zhou, J. Wu and Y. Tian, Series of C^N^C Cyclometalated Pt(II) Complexes: Synthesis, Crystal Structures, and Nonlinear Optical Properties in the Near-Infrared Region, *Inorg. Chem.*, 2018, 57, 14134–14143.
- 13 Z.-Z. Ma, Q.-H. Li, Z. Wang, Z.-G. Gu and J. Zhang, Electrically Regulating Nonlinear Optical Limiting of Metal-Organic Framework Film, *Nat. Commun.*, 2022, 13, 6347.
- 14 D.-J. Li, Q. Li, Z.-R. Wang, Z.-Z. Ma, Z.-G. Gu and J. Zhang, Interpenetrated Metal-Porphyrinic Framework for Enhanced Nonlinear Optical Limiting, *J. Am. Chem. Soc.*, 2021, 143, 17162–17169.
- 15 D.-J. Li, Q. Li, Z.-G. Gu and J. Zhang, Oriented Assembly of 2D Metal-Pyridylporphyrinic Framework Films for Giant Nonlinear Optical Limiting, *Nano Lett.*, 2021, 21, 10012– 10018.
- 16 Z.-B. Jin, G. Zhou, Y. Han, Z. Huang, Z.-G. Gu and J. Zhang, Topochemical Polymerization at Diacetylene Metal-Organic Framework Thin Films for Tuning Nonlinear Optics, J. Am. Chem. Soc., 2024, 146, 25016–25027.
- 17 Y.-H. Xiao, Z.-G. Gu and J. Zhang, Vapor-Assisted Epitaxial Growth of Porphyrin-Based MOF Thin Film for Nonlinear Optical Limiting, Sci. China: Chem., 2020, 63, 1059–1065.
- 18 Z.-K. Wang, M.-H. Du, P. Braunstein and J.-P. Lang, A Cutto-Link Strategy for Cubane-Based Heterometallic Sulfide Clusters with Giant Third-Order Nonlinear Optical Response, J. Am. Chem. Soc., 2023, 145, 9982–9987.
- 19 R. Ho-Wu, S. H. Yau and T. Goodson, Linear and Nonlinear Optical Properties of Monolayer-Protected Gold Nanocluster Films, ACS Nano, 2016, 10, 562–572.
- 20 Y. Liu, Q. Li, D. Li, X. Zhang, W. Fang and J. Zhang, Designable Al₃₂ –Oxo Clusters with Hydrotalcite–like Structures: Snapshots of Boundary Hydrolysis and Optical Limiting, *Angew. Chem., Int. Ed.*, 2021, **60**, 4849–4854.
- 21 J. Sun, X. Tang, Z.-H. Liu, Z. Xie, B. Yan, R. Yin, C. Chaolumen, J. Zhang, W. Fang, J. Wei and H. Shen, Labile Ligands Protected Cu₅₀ Nanoclusters with Tailorable Optical Limiting Effect, ACS Mater. Lett., 2024, 6, 281–289.

- 22 X. Sun, X. Yi, J. Zhang and L. Zhang, Sequential Aggregation of Heterometallic $\{M_4X_4\}$ -Cubanes to Wheel-Shaped In10 Ni $_8$ -Oxo Clusters for Optical Limiting Application, *Chem. Mater.*, 2023, 35, 5845–5853.
- 23 G.-K. Lim, Z.-L. Chen, J. Clark, R. G. S. Goh, W.-H. Ng, H.-W. Tan, R. H. Friend, P. K. H. Ho and L.-L. Chua, Giant Broadband Nonlinear Optical Absorption Response in Dispersed Graphene Single Sheets, *Nat. Photonics*, 2011, 5, 554–560.
- 24 D. Lu, J. Zhang, M. Deng, X. Liu, Z. Liu, K. Yin and H. Li, Impressive Nonlinear Optical Response of π-Conjugated, Photoluminescent Soft Nanoparticles in Polymer Matrix, *Carbon*, 2024, **230**, 119607.
- 25 B. Wang, B. Ma, K. Wang, H. Zhang, Z. Zhang, T. Song, S. Wang, M. Chen, S. Li, Q. Wang and H. Zhang, Fractal Growth of 2D NbSe₂ for Broadband Nonlinear Optical Limiting, *Adv. Funct. Mater.*, 2024, 34, 2401490.
- 26 N. Dong, Y. Li, Y. Feng, S. Zhang, X. Zhang, C. Chang, J. Fan, L. Zhang and J. Wang, Optical Limiting and Theoretical Modelling of Layered Transition Metal Dichalcogenide Nanosheets, Sci. Rep., 2015, 5, 14646.
- 27 A. Wang, J. Ye, M. G. Humphrey and C. Zhang, Graphene and Carbon–Nanotube Nanohybrids Covalently Functionalized by Porphyrins and Phthalocyanines for Optoelectronic Properties, Adv. Mater., 2018, 30, 1705704.
- 28 R. Liu, J. Hu, S. Zhu, J. Lu and H. Zhu, Synergistically Enhanced Optical Limiting Property of Graphene Oxide Hybrid Materials Functionalized with Pt Complexes, ACS Appl. Mater. Interfaces, 2017, 9, 33029–33040.
- 29 G.-J. Zhou and W.-Y. Wong, Organometallic Acetylides of PtII, AuI and HgII as New Generation Optical Power Limiting Materials, Chem. Soc. Rev., 2011, 40, 2541.
- 30 X. Yang, L. Yue, Y. Yu, B. Liu, J. Dang, Y. Sun, G. Zhou, Z. Wu and W. Wong, Strategically Formulating Aggregation–Induced Emission–Active Phosphorescent Emitters by Restricting the Coordination Skeletal Deformation of Pt(II) Complexes Containing Two Independent Monodentate Ligands, *Adv. Opt. Mater.*, 2020, 8, 2000079.
- 31 S. Zhu, J. Hu, S. Zhai, Y. Wang, Z. Xu, R. Liu and H. Zhu, AIPE-Active Pt(II) Complexes with a Tunable Triplet Excited State: Design, Mechanochromism and Application in Anti-Counterfeiting, *Inorg. Chem. Front.*, 2020, 7, 4677–4686.
- 32 Y. Cheng, D. Jiang, C. Xiao, M. Li, Y. Lin, C. Zhao, Z. Tang, H. Yin and W. Li, A Platinum Complex-Based Dimerized Electron Acceptor for Efficient Organic Solar Cells, *Adv. Energy Mater.*, 2025, 2404632.
- 33 Y.-S. Wong, M. Ng, M. C.-L. Yeung and V. W.-W. Yam, Platinum(II)-Based Host–Guest Coordination-Driven Supramolecular Co-Assembly Assisted by Pt···Pt and π – π Stacking Interactions: A Dual-Selective Luminescence Sensor for Cations and Anions, *J. Am. Chem. Soc.*, 2021, 143, 973–982.
- 34 B. Zhang, Y. Li, R. Liu, T. M. Pritchett, J. E. Haley and W. Sun, Extending the Bandwidth of Reverse Saturable Absorption in Platinum Complexes Using Two-Photon-

Initiated Excited-State Absorption, ACS Appl. Mater. Interfaces, 2013, 5, 565-572.

Research Article

- 35 H. Jia, B. Küçüköz, Y. Xing, P. Majumdar, C. Zhang, A. Karatay, G. Yaglioglu, A. Elmali, J. Zhao and M. Hayvali, Trans-Bis(Alkylphosphine) Platinum(II)-Alkynyl Complexes Showing Broadband Visible Light Absorption and Long-Lived Triplet Excited States, J. Mater. Chem. C, 2014, 2, 9720-9736.
- 36 A. Haque, L. Xu, R. A. Al-Balushi, M. K. Al-Suti, R. Ilmi, Z. Guo, M. S. Khan, W.-Y. Wong and P. R. Raithby, Cyclometallated Tridentate Platinum(II) Arylacetylide Complexes: Old Wine in New Bottles, Chem. Soc. Rev., 2019, 48, 5547-5563.
- 37 C.-L. Ho, Z.-Q. Yu and W.-Y. Wong, Multifunctional Polymetallaynes: Properties, Functions and Applications, Chem. Soc. Rev., 2016, 45, 5264-5295.
- 38 G.-J. Zhou, W.-Y. Wong, C. Ye and Z. Lin, Optical Power Limiters Based on Colorless Di-, Oligo-, Polymetallaynes: Highly Transparent Materials for Eye Protection Devices, Adv. Funct. Mater., 2007, 17, 963-975.
- 39 M. An, X. Yan, Z. Tian, J. Zhao, B. Liu, F. Dang, X. Yang, Y. Wu, G. Zhou, Y. Ren and L. Gao, Optimized Trade-Offs between Triplet Emission and Transparency in Pt(II) Acetylides through Phenylsulfonyl Units for Achieving Good Optical Power Limiting Performance, J. Mater. Chem. C, 2016, 4, 5626-5633.
- 40 G. G. Dubinina, R. S. Price, K. A. Abboud, G. Wicks, P. Wnuk, Y. Stepanenko, M. Drobizhev, A. Rebane and K. S. Schanze, Phenylene Vinylene Platinum(II) Acetylides with Prodigious Two-Photon Absorption, J. Am. Chem. Soc., 2012, 134, 19346-19349.
- 41 G. Zhou, W. Wong, S. Poon, C. Ye and Z. Lin, Symmetric Versus Unsymmetric Platinum(II) Bis(Aryleneethynylene)s with Distinct Electronic Structures for Optical Power Limiting/Optical Transparency Trade-off Optimization, Adv. Funct. Mater., 2009, 19, 531-544.
- 42 Z. Cai, M. Zhou, B. Li, Y. Chen, F. Jin and J. Huang, Investigation of Photophysical Properties of New Branched Compounds with Triazine and Benzimidazole Units, New J. Chem., 2014, 38, 3042.
- 43 R. L. Roberts, T. Schwich, T. C. Corkery, M. P. Cifuentes, K. A. Green, J. D. Farmer, P. J. Low, T. B. Marder, M. Samoc and M. G. Humphrey, Organometallic Complexes for Nonlinear Optics. 45. Dispersion of the Third-Order Nonlinear Optical Properties of Triphenylamine-Cored Alkynylruthenium Dendrimers, Adv. Mater., 2009, 21, 2318-2322.
- 44 X. Yang, B. Jiao, J.-S. Dang, Y. Sun, Y. Wu, G. Zhou and W.-Y. Wong, Achieving High-Performance Solution-Processed Orange OLEDs with the Phosphorescent Cyclometalated Trinuclear Pt(II) Complex, ACS Appl. Mater. Interfaces, 2018, 10, 10227-10235.
- 45 L. Zhang, M. Morshedi and M. G. Humphrey, Outstanding Multi-Photon Absorption at π-Delocalizable Metallodendrimers, Angew. Chem., Int. Ed., 2022, 61, e202116181.

- 46 C. Yao, Z. Tian, D. Jin, F. Zhao, Y. Sun, X. Yang, G. Zhou and W.-Y. Wong, Platinum(II) Acetylide Complexes with Star- and V-Shaped Configurations Possessing Good Tradeoff between Optical Transparency and Optical Power Limiting Performance, J. Mater. Chem. C, 2017, 5, 11672-11682.
- 47 Z. Chen, A. K.-W. Chan, V. C.-H. Wong and V. W.-W. Yam, A Supramolecular Strategy toward an Efficient and Selective Capture of Platinum(II) Complexes, J. Am. Chem. Soc., 2019, **141**, 11204-11211.
- 48 Y.-F. Zhong, H. Zhang, G. Mu, W.-T. Liu, Q. Cao, C.-P. Tan, L.-N. Ji and Z.-W. Mao, Nucleus-Localized Platinum(11)-Triphenylamine Complexes as Potent Photodynamic Anticancer Agents, Inorg. Chem. Front., 2019, 6, 2817-2823.
- 49 T. Yasuda, T. Shimizu, F. Liu, G. Ungar and T. Kato, Electro-Functional Octupolar π-Conjugated Columnar Liquid Crystals, J. Am. Chem. Soc., 2011, 133, 13437-13444.
- 50 W. Yang, A. Karatay, J. Zhao, J. Song, L. Zhao, Y. Xing, C. Zhang, C. He, H. G. Yaglioglu, M. Hayvali, A. Elmali and Near-IR Broadband-Absorbing Trans-Küçüköz, Bisphosphine Pt(II) Bisacetylide Complexes: Preparation and Study of the Photophysics, Inorg. Chem., 2015, 54, 7492-7505.
- 51 J. Lu, Q. Pan, S. Zhu, R. Liu and H. Zhu, Ligand-Mediated Photophysics Adjustability in Bis-Tridentate Ir(III) Complexes and Their Application in Efficient Optical Limiting Materials, Inorg. Chem., 2021, 60, 12835-12846.
- 52 J. M. Keller, K. D. Glusac, E. O. Danilov, S. McIlroy, P. Sreearuothai, A. R. Cook, H. Jiang, J. R. Miller and K. S. Schanze, Negative Polaron and Triplet Exciton Diffusion in Organometallic "Molecular Wires", J. Am. Chem. Soc., 2011, 133, 11289-11298.
- 53 W. He, M. Y. Livshits, D. A. Dickie, Z. Zhang, L. E. Mejiaortega, J. J. Rack, Q. Wu and Y. Qin, "Roller-Wheel"-Type Pt-Containing Small Molecules and the Impact of "Rollers" on Material Crystallinity, Electronic Properties, and Solar Cell Performance, J. Am. Chem. Soc., 2017, 139, 14109-14119.
- 54 Z. Yin, X. Chang, J. Zang, S. Lin, Z. Zhou, T. Liu, L. Ding, H. Peng and Y. Fang, A Triphenylamine-Based Pt(II) Metallacage via Coordination-Driven Self-Assembly for Nonlinear Optical Power Limiting, J. Mater. Chem. C, 2022, 10, 10429-10438.
- 55 Y. Du, N. Dong, M. Zhang, B. Jiang, N. Sun, Y. Luo, S. Zhang, G. Wang and J. Wang, Poly(Arylene Ether)s Based on Platinum(II) Acetylide Complexes: Synthesis and Photophysical and Nonlinear Absorption Properties, J. Mater. Chem. C, 2018, 6, 7317-7325.
- 56 J. Wang, J. Zhao, S. Han, Y. Li, W. Zeng, J. Sun and S. Zhou, Significant Enhancement of Reverse Saturable Absorption Ability via Pt(II) Incorporation into the Conjugated Backbone of Benzo[1,2-b:4,5-b']Dithiophene-Based Donor-Acceptor Copolymers, Macromolecules, 2024, 57, 1030-1037.
- 57 M. Zhang, X. Xu, J. Liu, Y. Jiang, J. Wang, N. Dong, C. Chen, B. Zhu, Y. Liang, T. Fan and J. Xu, All-Organic

- Composite Films for High Flexibility and Giant Nonlinear Optical Limiting Responses, *ACS Appl. Mater. Interfaces*, 2022, **14**, 33787–33796.
- 58 F. Xing, J. Wang, Z. Wang, Y. Li, X. Gou, H. Zhang, S. Zhou, J. Zhao and Z. Xie, Covalently Silane-Functionalized Antimonene Nanosheets and Their Copolymerized Gel Glasses for Broadband Vis-NIR Optical Limiting, ACS Appl. Mater. Interfaces, 2021, 13, 897-903.
- 59 W. Feng, K. Liu, J. Zang, G. Wang, R. Miao, L. Ding, T. Liu, J. Kong and Y. Fang, Flexible and Transparent Oligothiophene-o-Carborane-Containing Hybrid Films for Nonlinear Optical Limiting Based on Efficient Two-Photon Absorption, ACS Appl. Mater. Interfaces, 2021, 13, 28985–28995.
- 60 Z. Xie, F. Wang and C. Liu, Organic-Inorganic Hybrid Functional Carbon Dot Gel Glasses, *Adv. Mater.*, 2012, 24, 1716–1721.
- 61 A. A. Noble, I. H. Joe and S. Nazar, Defect-Controlled Fabrication of Reduced Graphene Oxide/ZnO/PMMA-Based Solid-State Optical Limiting Filters with SA/RSA Switching Property, *Carbon*, 2024, 228, 119435.
- 62 J.-W. Li, W. Dong, Y. Liu, Y. Li, L.-Y. Qiao, G.-L. Liu, H. Zhang, C. Wang, H.-L. Zheng and J.-Q. Zhao, Water-Stable Zero-Dimensional Hybrid Zinc Halide Modulated by π-π Interactions: Efficient Blue Light Emission and Third-Order Nonlinear Optical Response, *Inorg. Chem. Front.*, 2024, 11, 8431–8438.

- 63 L.-S. Wang, Y. Wang, C.-L. Lv, C. Guo, F.-Y. Xing, Y.-J. Dong, Z. Xie, S.-Y. Zhou and Y.-G. Wei, Polyoxometalates with Tunable Third-Order Nonlinear Optical and Superbroadband Optical Limiting Properties, *Inorg. Chem. Front.*, 2022, 9, 4413–4424.
- 64 B. Han, B. Liang, E. Zhang, J. Li, Y. Li, Q. Zhang, Z. Xie, H. Wang and J. Jiang, Phthalocyanine Covalent Organic Frameworks: Dimensionality Effect on Third-Order Nonlinear Optical Properties, Adv. Funct. Mater., 2024, 34, 2404289.
- 65 J. Wei, F. Hu, C. Lv, L. Bian, X. Quan and Q. Ouyang, Fabrication of Dual-Functional MXene@NiCo₂S₄ Composites with Enhanced Nonlinear Optical and Electrochemical Properties, Small, 2025, 21, 2411146.
- 66 M. Shi, N. Dong, N. He, Y. Wan, H. Cheng, M. Han, J. Wang and Y. Chen, MoS₂ Nanosheets Covalently Functionalized with Polyacrylonitrile: Synthesis and Broadband Laser Protection Performance, *J. Mater. Chem.* C, 2017, 5, 11920–11926.
- 67 S.-T. Wang, X. Qi, R.-Q. Chen, W.-H. Fang and J. Zhang, Two Solvent-Dependent Al₁₆ Nanorings: Design, Synthesis and Nonlinear Optical Limiting Behavior, *Inorg. Chem. Front.*, 2024, **11**, 462–469.
- 68 S. Wang, Y. Liu, C. Feng, W. Fang and J. Zhang, The Largest Aluminum Molecular Rings: Phenol-thermal Synthesis, Photoluminescence, and Optical Limiting, *Aggregate*, 2023, 4, e264.